Effects of anatase TiO2 morphology and surface fluorination on environmentally relevant photocatalytic reduction and oxidation reactions

Effects of the TiO_2 Morphology and Surface Fluorination on the Photocatalytic Cr(VI) Reduction and Rhodamine B Oxidation Reactions

Maria Vittoria Dozzi[a,*], Marco Montalbano[a], Gianluigi Marra[b], Lorenzo Mino,[c] Elena Selli[a]

[a] *Dipartimento di Chimica, Università degli Studi di Milano, via C. Golgi 19, I-20133 Milano, Italy*

[b] *Eni S.p.A Renewable Energy, Magnetic Fusion and Material Science Research Center (DE-R&D), via G. Fauser 4, I-28100 Novara, Italy*

[c] *Dipartimento di Chimica and NIS Centre, University of Torino, via P. Giuria 7, I-10125 Torino, Italy*

A B S T R A C T

Aiming at clarifying the interplay between surface fluorination and particle morphology on the TiO_2 photoactivity, the photocatalytic activity of anatase nanocrystals, characterized by a pseudo-spherical shape or a nanosheet structure, is investigated in both a reduction and an oxidation reaction, either in the absence or in the presence of added fluoride anions. Cr(VI) photoreduction appears to be strongly favored by a larger exposure of {001} facets, though further addition of F^- ions leads to a systematic decrease of photoactivity. More interestingly, a clear beneficial synergistic effect induced by the plate-like anatase TiO_2 morphology and its surface fluorination is clearly outlined in Rhodamine B degradation, possibly resulting from the intrinsic ability of F-{001} facets of boosting $^{\bullet}OH$ radical mediated oxidation paths.

Keywords: plate-like TiO_2, {001} facets, surface fluorination, Cr(VI) reduction, Rhodamine B degradation

* Corresponding author.
E-mail address: mariavittoria.dozzi@unimi.it (M.V. Dozzi).

1 INTRODUCTION

The design and synthesis of cost effective, efficient and scalable TiO_2-based materials able to convert light into chemical energy through photocatalytic processes is a key challenge for a sustainable energy economy. A wide variety of synthetic routes has been developed to prepare TiO_2 in different forms and shapes, with different surface area and porosity [1–3], and to improve its photocatalytic activity, either by enhancing light absorption [4–7] or by improving the separation of photoproduced charge couples [8–10].

In particular, shape-controlled anatase TiO_2 has been prepared mainly by adding capping agents during the synthesis, which may preferentially stabilize the {001} facets during the crystal growth, with the production of nanocrystals with a plate-like shape (see Scheme 1) [11–14]. Such facets, though thermodynamically less stable, are expected to be more reactive with respect to the dominant {101} ones, mainly due to a high density and a very strained configuration of surface undercoordinated Ti atoms. Moreover, by tailoring the truncation degree of anatase crystals, the overall photoactivity may be further increased as a direct consequence of the selective migration of photogenerated holes towards the {001} facets and of photopromoted electrons to the {101} ones [15].

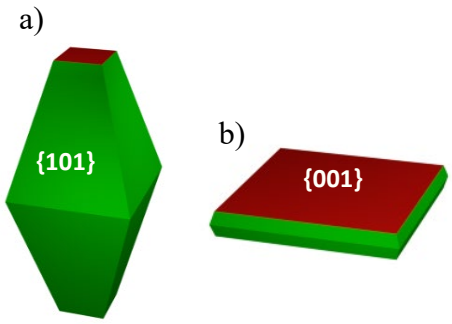

Scheme 1. (a) equilibrium crystal shape and (b) platelet-like morphology of anatase crystal with the indication of the types of exposed facets.

At the same time, another strategy that may be pursued to improve the photocatalytic performance of TiO_2 consists in the *in-situ* surface fluorination [16–19], implying a simple ligand exchange reaction between fluoride anions and surface hydroxyl groups (at acidic pH):

$$\equiv \mathrm{Ti} - \mathrm{OH} + \mathrm{F}^- \rightarrow \equiv \mathrm{Ti} - \mathrm{F} + \mathrm{OH}^- \quad (1)$$

This method was found to induce different effects on photocatalysis, depending not only on the main degradation paths of different substrates [20], but also on the surface area and phase composition of TiO_2 [21].

On the other hand, fluoride anions are often used as capping agents in the synthesis of shape controlled anatase [22–28] and the effects on photoactivity arising from residual surface fluorination are very difficult to be distinguished from those deriving from the morphology of such materials. Indeed, plate-like materials are usually synthesized in the presence of a higher fluoride ions concentration with respect to spherically shaped TiO_2 materials [13,15,29]. The different amount of residual adsorbed fluoride anions for the two morphologies does not allow to appreciate if the effects on photoactivity induced by surface fluorination may synergistically cooperate with morphology control in boosting the photoactivity of TiO_2-based materials [15].

In the present work we investigate the effects that TiO_2 surface fluorination has on photocatalytic oxidation and reduction reactions in relation to the amount of exposed anatase {001} facets. Fluorine-free TiO_2 materials with differing morphologies were obtained through post-synthesis washing to efficiently remove the capping agent. Such materials were eventually successively *in-situ* re-fluorinated. Under such conditions the home-made photocatalysts were systematically tested in both Rhodamine B photobleaching and Cr(VI) reduction, proceeding through completely different mechanistic routes [30–32]. These two model test reactions find an important application of photocatalysis as innovative and clean/environmentally friendly technology for industrial wastewaters decontamination [33–38]. In fact, hexavalent Cr(VI) ions, notoriously toxic and carcinogenic [39] and generally released in effluents by various

industrial activities (*e.g.* electroplating, leather tanning, textile production, steel fabrication), can be efficiently converted by photocatalytic reduction on semiconductors into Cr(III) species, exhibiting lower toxicity and mobility in the environment [40]. At the same time, the demand for Rhodamine B (RhB) conversion into harmless chemicals has also started growing in the recent years, due to the increased use of xanthene-derived dyes in food, paper, textile and leather industry. The undesired presence of RhB (see Scheme 2) in waters and food represents a serious threat for the human health due to the dye ability of causing injury to human skin, eyes, respiratory system as well as being potentially carcinogenic and neurotoxic [41,42]. Rhodamine B decomposition is thus highly required also to gain a sustainable recycling of industrial wastewaters.

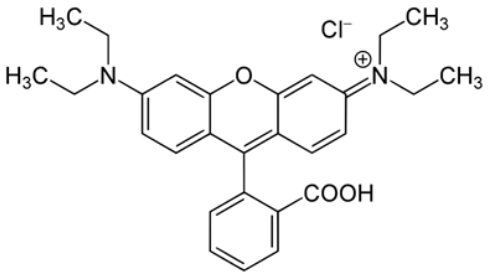

Scheme 2: Rhodamine B (RhB)

2 EXPERIMENTAL SECTION

2.1 Photocatalyst preparation

Differently shaped TiO_2 samples, characterized by a pseudo-spherical shape or a nanosheet structure, were prepared through the hydrothermal route by employing titanium isopropoxide as Ti precursor and HF as capping agent [29,43]. In particular, a fixed amount of titanium isopropoxide (10 mL) was mixed under stirring for 15 min in a Teflon liner with different volumes of a 48 wt% HF solution and different amounts of water (see Table 1) up to a 11.2 mL final volume. A reference sample was prepared under the same conditions by simply adding 1.2 mL of water (and no HF) to titanium isopropoxide.

The liner was then transferred into a closed stainless-steel autoclave to be heated at 180 °C for 24 h. The obtained precipitate was recovered after cooling the autoclave down to room temperature using a stream of compressed air. A series of washing cycles with ultrapure Milli-Q water followed, up to a fluoride ion concentration in the supernatant, detected by means of ionic chromatography (Methrohm 761 compact IC with conductivity detector), below 5 ppm. The solid was then collected, dried in an electric oven at 70 °C overnight, and grounded into the form of fine powders by means of an agate mortar. The so-obtained materials were labelled as HT_X, where HT refers to the employed preparation method (hydrothermal procedure) and X stands for the nominal F/Ti ratio employed during the synthesis, *i.e.* 0.1 or 1.0. The reference sample was labelled as HT_0, as no fluorine was used during its synthesis.

In order to remove the residual fluorine on the materials' surface, a portion of each sample underwent washing cycles with an aqueous NaOH solution. During the washing procedure, a fixed amount of photocatalyst (1.0 g) was dispersed in 200 cm^3 of a 0.1 M NaOH aqueous solution by means of a 30 min ultrasonic treatment. The suspension was then left stirring in the dark for 1 h at 60 °C, followed by a 10 h-long stirring in the dark at room temperature [44]. The powders were then recovered by centrifugation and washed several times (maximum six

times) with Milli-Q water (200 cm^3) up to neutral pH of the suspension and finally dried at 70 °C overnight. The so-obtained washed samples were labelled as HT_X_NaOH.

Table 1: Amounts of HF aqueous solution (48 wt%) and of ultrapure H_2O employed in the hydrothermal synthesis of the photocatalysts.

Sample	HF Volume / cm^3	H_2O Volume / cm^3
HT_0	-	1.200
HT_0.1	0.120	1.080
HT_1	1.200	-

All reagents were purchased from Sigma-Aldrich and employed as received. Water purified by a Milli-Q water system (Millipore) was used throughout.

2.2 Photocatalysts characterization

X-Ray Powder Diffraction (XRPD) patterns were acquired using a Panalytical X'Pert Pro diffractometer, using Ni-Filtered Cu K_α radiation (λ=1.54056 Å) at a scan rate of 0.05 degree s^{-1}. The relative amount of exposed {001} facets of the full anatase samples was calculated by applying a Rietveld-based approach on diffraction data [45]. Phase composition analysis was performed using the Quanto software [46].

Specific surface area (SSA) of the samples was obtained by measuring N_2 adsorption/desorption isotherms at liquid nitrogen temperature according to the Brunauer-Emmet-Teller (BET) method in a Micrometrics Tristar II 3020 V1.03 apparatus equipped with an ASAP 2020 surface area and porosity analyzer, after outgassing at 150 °C for 2 h under constant nitrogen flux. SSA data were calculated by the instrument provided software starting from the linear region of the BET isotherm, using the linearized form of the BET equation.

UV-Visible absorption spectra of the materials in powder form were acquired in diffuse reflectance mode (DR spectra) using a Jasco V-670 spectrophotometer equipped with a PIN-757 integrating sphere, using barium sulphate as a reference standard. Reflectance (R) spectra

in the 200-800 nm region, with a 1 nm spectral resolution, were converted into absorption (A) spectra using the relation A = 1 – R.

HRTEM analysis was carried out with a JEOL JEM 2010 electron microscope, equipped with a LAB6 electron gun operating at 200 keV and a Gatan CCD camera allowing high-resolution imaging. Specimens for HRTEM analysis were sonicated in 2-propanol and then transferred as a suspension to a copper grid covered with a holey carbon film. Micrographs were taken after solvent evaporation, spanning over the whole region of the sample, to achieve a truly representative statistical mapping of the investigated materials.

Thermogravimetric Analysis (TGA) were carried out on a Mettler-Toledo TGA/DSC 2 STARe system. Thermograms were recorded in the 30-800 °C temperature range, with a heating ramp of 10 °C min^{-1} under a 50 cm^3 min^{-1} air flux.

X-Ray photoemission spectra (XPS) were recorded on a M-Probe apparatus, Surface Science Instruments, equipped with an Al-K_α monochromatic radiation X-Ray source (1486.6 eV photon energy). XPS surveys were recorded in a binding energy range from 1000 to 0 eV and peak shift correction was applied using the adventitious carbon C1s signal at 284.6 eV as internal reference.

For Fourier-transform infrared (FT-IR) spectroscopy measurements the samples were pressed in self-supporting pellets ("optical density" of ca. 10 $mg \cdot cm^{-2}$) and placed in quartz cells equipped with KBr windows designed to carry out spectroscopic analysis in controlled atmosphere. The thermal treatments at increasing temperatures (150, 300 and 500 °C) were performed for 90 min under dynamic vacuum (residual pressure < 1×10^{-4} mbar). At the end of each treatment step, the samples were contacted with O_2 at 10 mbar to restore the stoichiometry of the TiO_2. The spectra were obtained using a Bruker Equinox 55 spectrometer with a resolution of 2 cm^{-1} and averaging 64 scans. The optical density of the pellets was employed to normalize all the acquired spectra.

2.3 Photocatalytic activity in the absence or upon in-situ addition of fluorides

The photocatalytic activity of home-made samples was tested in aqueous suspensions, employing the dye Rhodamine B (RhB) or dichromate ($Cr_2O_7^{2-}$) ions as organic or inorganic degradation substrates, respectively. The photostability of both substrates in aqueous solution was preliminarily verified under the adopted irradiation conditions.

All photocatalytic degradation runs were performed under atmospheric conditions in a magnetically stirred 100 mL reactor, inserted in a home-made housing consisting in a black box mounted on optical bench. The irradiation source was an Osram, model Powerstar HCI-T, 150 W/NDL lamp, mounted on a Twin Beam T 150 R reflector, mainly emitting visible light above 400 nm, with a small emission in the 350–400 nm range and an average full emission intensity on the reactor of *ca.* 120 mW cm^{-2}, as regularly checked with an optical power meter (Thorlabs PM200) equipped with a thermal power sensor (Thorlabs S302C). A 285 nm cut off filter was mounted at the black box entrance. The lamp and the reactor were separated by a fixed distance of 10 cm. The whole set up was maintained at ambient temperature by a continuous stream of air.

In all kinetic runs, the TiO_2 content of the irradiated aqueous suspensions was 0.1 g L^{-1}. Aqueous TiO_2 suspensions were preliminary treated with ultrasound for 30 min in order to ensure the de-aggregation of the photocatalyst particles, prior to the addition of an aqueous solution containing the organic or inorganic substrate. So-called natural pH conditions were obtained by this way. When required, the pH was adjusted down to *ca.* 3.7 by adding small amounts of a concentrated $HClO_4$ aqueous solution. $HClO_4$ was chosen because of the low affinity of ClO_4^- anions for TiO_2 [47]. To attain *in-situ* surface fluorination of the photocatalyst, fluoride ions, able to very quickly displace the -OH groups on the surface of titanium dioxide, were then added to the suspensions in the form of NaF, prior to the addition of the substrates [20]. The overall fluoride concentration was fixed in order to gain a F/Ti molar ratio in aqueous

suspension equal to 0.1 and 2 for the Cr(VI) photoreduction and Rhodamine B photodegradation, respectively.

Then, appropriate volumes of stock solutions containing Cr(VI) or RhB were added to fix the initial concentration of the photocatalytic reaction substrates in the aqueous suspensions at the following values: 3.3×10^{-5} M for Cr(VI), from a solution obtained by dissolving $K_2Cr_2O_7$ in water, and 1.0×10^{-5} M for RhB. Before starting irradiation, the so obtained suspensions were magnetically stirred in the dark for 15 min to attain the adsorption equilibrium of the substrates on the photocatalyst surface.

Stirring was continued during the runs. The lamp was always switched on at least 30 min before the beginning of irradiation. At different time intervals during the runs, 5 mL of the suspension were withdrawn from the reactor and centrifuged employing an EBA-20 Hettich centrifuge. The supernatant was analyzed colorimetrically for Cr(VI) residual content, using the 1,5-diphenylcarbazide method [48]. RhB photobleaching was monitored during the runs by spectrophotometric analysis at 553 nm, the maximum of RhB absorption. According to calibration the molar extinction coefficient of the dye at this wavelength is $\varepsilon = (9.92 \pm 0.02) \times 10^4$ M^{-1} cm^{-1}.

All kinetic runs were performed up to *ca.* 70% substrate removal and repeated at least twice, to check their reproducibility. The initial pH of the suspensions was fixed at pH 3.7 for all the performed Cr(VI) photocatalytic reduction kinetic runs, *i.e.* the pH decrease allowing a beneficial shift of the reduction potential of the Cr(VI)/Cr(III) couple toward more positive value with respect to the TiO_2 conduction band edge [49].

2.4 Substrates adsorption measurements on TiO_2 and fluorinated TiO_2

Aiming at investigating the substrates affinity for the different photocatalysts, adsorption tests were performed at pH 3.7, both in the presence and in the absence of NaF, under the same experimental conditions adopted during the photocatalytic runs, except for the amount of TiO_2,

which was fixed at 1.0 g L^{-1}. The suspensions were kept under stirring in the dark and samples were withdrawn after 15 min, 60 min and 180 min, centrifuged and analyzed for determining the Cr(VI) and/or RhB residual amount in the supernatant. Adsorption equilibrium was attained in 15-30 min, though the adsorption data after 3 h-long equilibration were considered as most reliable, as in previous studies [50].

3 RESULTS AND DISCUSSION

3.1 Photocatalyst characterization

XRPD diffractograms of all samples of the HT_X series were recorded to investigate both phase composition and morphology of the materials. As shown in Figure 1 all diffraction patterns perfectly matched those of pure anatase.

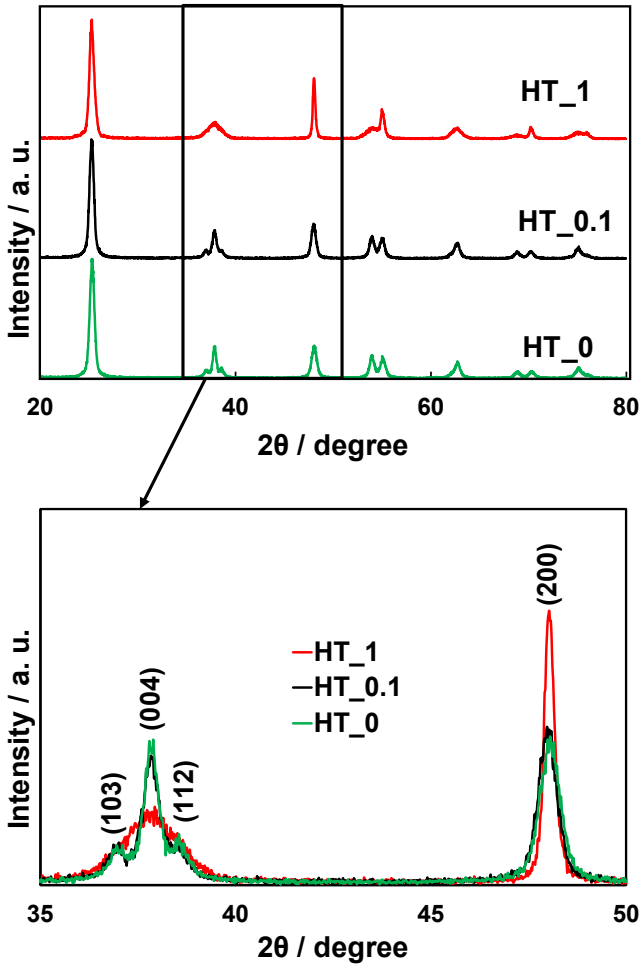

Figure 1: XRPD patterns of samples of the HT_X series evidencing (103), (004), (112), and (200) anatase reflections.

Quantitative phase analysis (Table 2), performed through Rietveld refinement [51] showed that rutile or brookite content was non-detectable, nor appreciable presence of other phases such as $TiOF_2$ was observed, indicating that the samples were composed of pure anatase independently of the amount of fluorine employed during the synthesis. With increasing fluorine content the width of reflections with ($l>h,k$) broadened, accompanied by a shrinking of the peaks characterized by a strong h component, in the 35-50° 2θ range, indicating a change in crystal growth along specific crystallographic directions [29].

The nanoparticles size and the relative amount of exposed {001} facets, in the different samples, calculated by applying a Rietveld-based XRPD approach [45], are collected in Table 2. The so obtained values clearly demonstrate that the anatase {001} facets percentage increased by increasing the HF amount during the synthesis, *i.e.* passing from *ca.* 15% for HT_0.1 to 65% for HT_1. The latter sample incontrovertibly consisted of plate-like nanocrystals, as confirmed by the HR-TEM images reported in Figure 2a,b. In line with previous findings [29], the plate-like crystals of HT_1 appeared piled up face-to-face, one above the other, thus minimizing the total surface energy [28,52]. On the contrary, the casual distribution of particles displayed by HT_0.1 aggregates (Figure 2b) is coherent with an isotropic shape of crystals (Figure 2a).

Table 2: Average nanoparticles thickness and width, percentage of {001} facets exposure, BET specific surface area (SSA) and residual carbonaceous content detected by TGA analysis of the synthesized pure anatase materials.

Sample	thickness / nm	width / nm	{001} (%)	SSA (m^2 g^{-1})	Total carbon loss (%)
HT_0	21.4(4)	14.6(2)	7.2(6)	93(1)	4
HT_0.1	17.2(3)	16.8(3)	14.8(8)	78(1)	5
HT_1	7.8(2)	39(1)	67(2)	84(4)	6
HT_0.1_NaOH	18.5(8)	16.5(7)	14.0(2)	82(2)	5
HT_1_NaOH	8.2(2)	38(1)	65(1)	82(7)	5

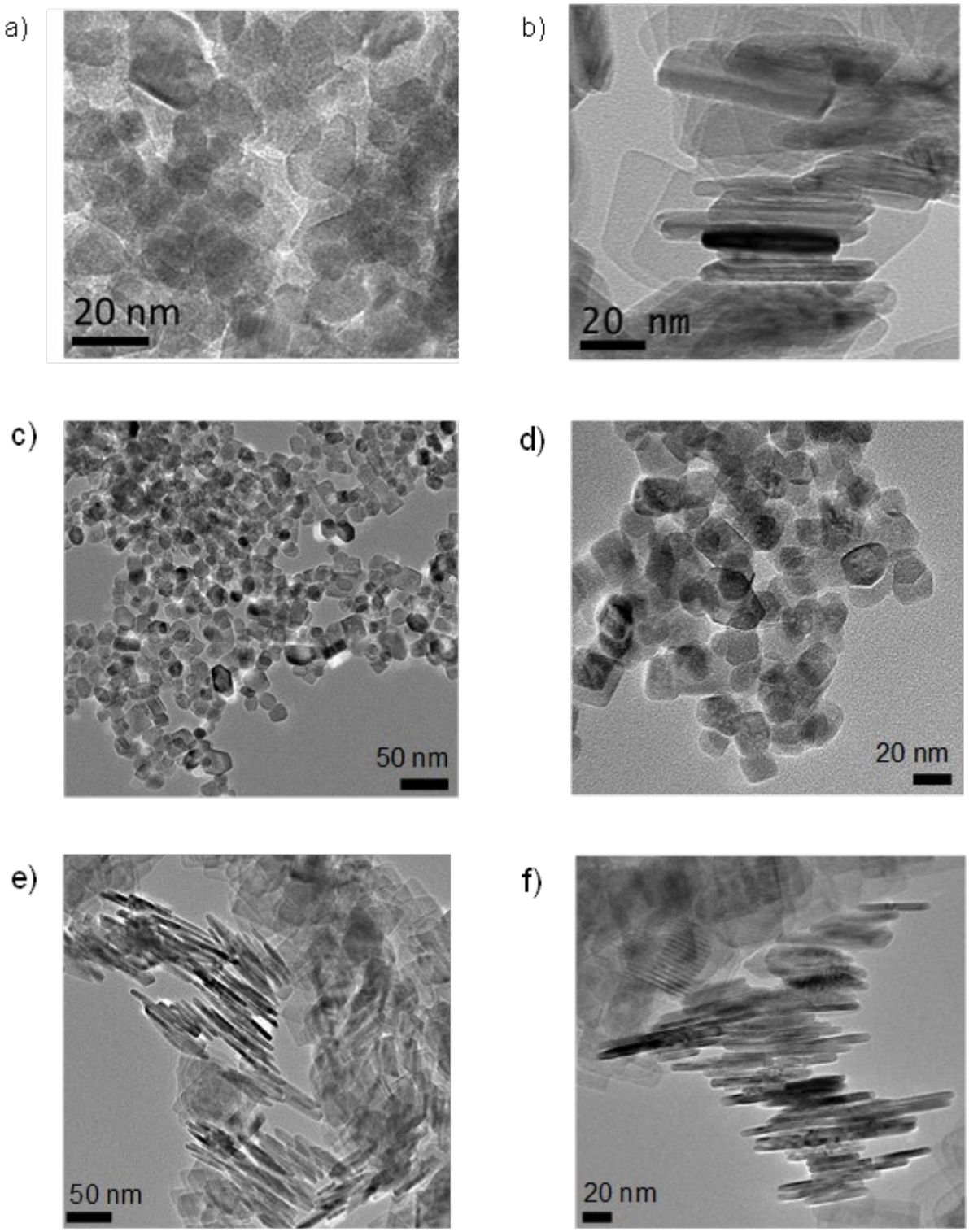

Figure 2: HRTEM images of (a) HT_0.1, (b) HT_1, (c, d) HT_0.1_NaOH and (e, f) HT_1_NaOH samples.

At the same time, HR-TEM images further confirmed both crystal thickness and width values of platelet-like HT_1 nanoparticles, calculated from XRPD data [45] and corresponding to *ca.* 8 and 40 nm, respectively, as reported in Table 2. More interestingly, the capping agent

removal procedure did not significantly alter the percentage of exposed {001} facets in any of the investigated materials (Table 2), *i.e.* the specific TiO_2 crystal shape being entirely preserved even after the samples washing (Figure 2c-f).

BET analysis confirmed similar SSA in the 82-93 m^2 g^{-1} range, for both HT_X and HT_X_NaOH series samples, except for the reference HT_0, synthesized in the absence of fluoride anions, having a slightly higher SSA (Table 2). Moreover, no significant variation in SSA was observed upon washing. Thus, the photocatalytic activities of the materials can be directly compared, all of them having the same SSA.

Diffuse Reflectance UV-Vis absorption spectra of the investigated samples are characterized by a very marked absorption onset for $\lambda < 400$ nm, similar to that of pure anatase (see Fig. 3). The absorption onset was found to be independent of the F/Ti ratio employing during the synthesis, *i.e.* it is unaffected by the relative amount of exposed crystal facets (see inset of Fig. 3). In the literature the anatase band gap has been reported to be red- [53–55], blue- [29,56] shifted or unmodified [57,58] by an increase in the {001} facets content. Moreover, the washing procedure did not produce any absorption edge variation for any of the prepared sample, thus resulting in an overall preservation of the original optical properties also upon the application of the here adopted fluorine removal treatment (see Fig. 3).

UV-vis absorption spectra did not evidence the presence of any residual carbonaceous impurities adsorbed on the materials surface (which are generally known to cause the appearance of continuous absorption in the visible region of TiO_2 DR spectra [59]), in line with the finding that pretty similar percentages of total mass losses were obtained by thermogravimetric analysis (TGA) of all samples (see Table 2).

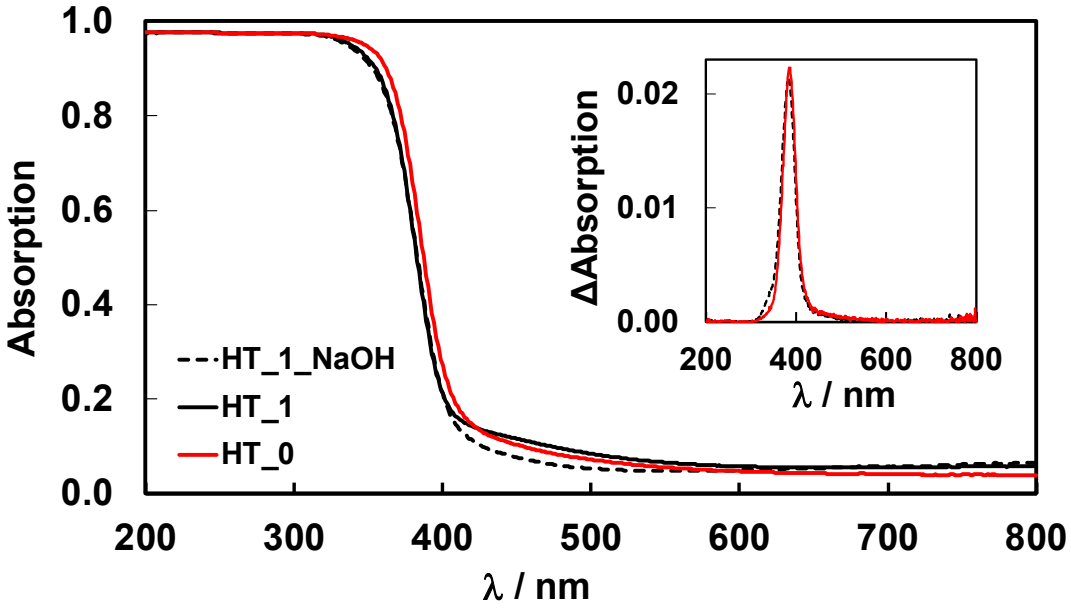

Figure 3: Absorption spectra of HT_X and HT_X_NaOH series samples. Inset: DRS spectra numerical first derivative of HT_X_NaOH samples highlights invariance of the absorption band edge upon the change of titania morphology.

The surface chemical composition of the home-made samples was assessed *via* XPS analysis (Figure 4).

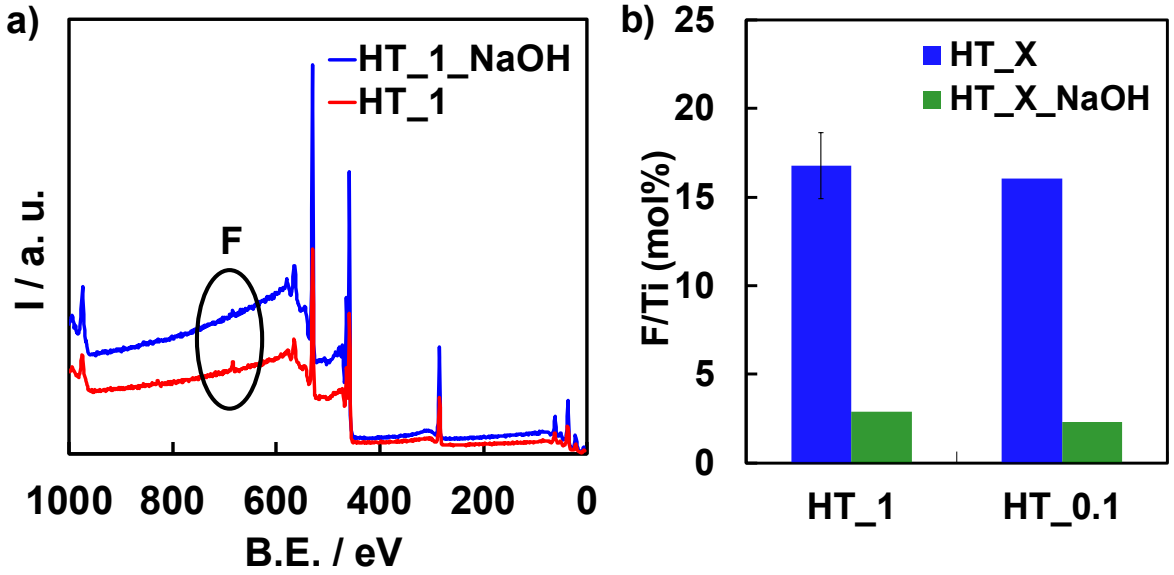

Figure 4: (a) XPS survey spectra and (b) quantitative surface F/Ti molar percentages obtained for the HT_X and HT_X_NaOH samples. As highlighted in panel (a) surface fluoride ions signal is located at 684 eV.

Titanium, carbon and oxygen were identified in XPS spectra by the signals binding energies (BE) at *ca.* 458.8 eV (Ti2p), 531 eV (O1s) and 284.5 eV (C1s), respectively. Spectra of HT_1 and HT_0.1 also show a small peak at binding energy 684 eV [60,61], attributed to F1s, indicating the residual presence of fluoride anions on the surface of the original materials. No XPS signal at 688 eV, assigned to substitutional F ions in the TiO_2 lattice, was detected, possibly always being below the detection limit of the XPS technique [29,62].

As reported in Figure 4b, quantitative XPS analysis demonstrated the effective (though not complete) removal of the residual F capping agent from HT_1 and HT_0.1 by the here applied post-synthesis washing procedure. In fact, the overall surface F/Ti ratios passed from *ca.* 16% to *ca.* 2% in the washed samples.

3.2 Cr(VI) adsorption and photocatalytic reduction

The effects induced on Cr(VI) adsorption on the investigated samples by the *in-situ* surface fluorination and by the TiO_2 morphology can be appreciated in Figure 5, reporting the relative percent amounts of Cr(VI) adsorbed on HT_0.1_NaOH and HT_1_NaOH, both in the absence (blue) and in the presence (yellow) of fluoride ions at pH 3.7.

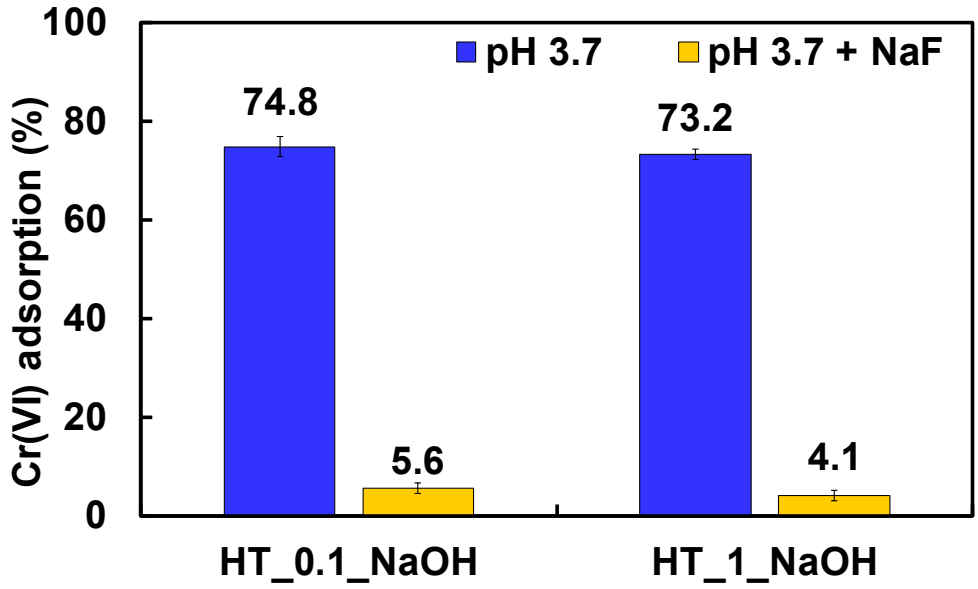

Figure 5: Percent amount of adsorbed Cr(VI) onto HT_0.1_NaOH and HT_1_NaOH after 180 min stirring in the dark at pH 3.7 in the absence of fluoride ions (blue) and under *in-situ* fluorinated conditions with a F/Ti ratio equal to 0.1 at the same pH (yellow).

The adsorption of dichromate species is strongly hampered upon *in-situ* surface fluorination on both materials, even for the relatively low F/Ti molar ratio here employed (corresponding to 0.1). In fact, in the absence of fluoride anions, the surface of titanium dioxide is rich in surface bound terminal $\equiv Ti-OH$ groups, which play a key role in ensuring dichromate adsorption on TiO_2 by means of surface complexation [63]. Moreover, at pH 3.7, the titanium dioxide surface is expected to be positively charged, this pH being below the zero charge (pH_{pzc}) of TiO_2, generally located for TiO_2-based materials at pH 5.6 [64]. These combined effects of course allow for a fast and significant (almost quantitative) adsorption of negatively charged $Cr_2O_7^{2-}$ anions on TiO_2 surface [30,65]. Differently, the *in-situ* fluorination implies the formation of stable $\equiv Ti-F$ termination on the TiO_2 surface, with a consequent shift of the surface charge towards more negative values, which hinders the dichromate anions adsorption on the surface of titanium dioxide [66], as evidenced in Figure 5.

In the absence of light, both HT_0.1_NaOH and HT_1_NaOH samples are equally able to adsorb dichromate ions. So the relative percent amounts of the inorganic anionic species adsorbed on the investigated TiO_2 photocatalysts seems not to be affected by the relative {001} facets exposure, nor in the absence or in the presence of *in-situ* added fluoride ions.

The activity of the here investigated TiO_2 samples in Cr(VI) photocatalytic reduction can be compared in terms of first order rate constants, measured either in aqueous suspensions at pH 3.7 (k_{ac}) and at pH 3.7 in the presence of fluoride anions (*in-situ* fluorinated surface, k_F), as shown in Figure 6.

Firstly, among the HT_X_NaOH samples, *i.e.* showing different relative percentage of clean {001} facets, the plate-like material is by far the best photocatalyst, with an activity double to that of commercial benchmark P25 TiO_2 (for which $k_{ac} = 3.3 \cdot 10^{-4}$ s^{-1}).

Interestingly, the outstanding photoactivity attained by increasing the percentage of exposed {001} TiO_2 facets, *i.e.* the k_{ac} attained with the HT_1_NaOH being three-time greater than that

obtained with HT_0.1_NaOH, cannot be explained by taking into account the similar dichromate anions adsorption under dark conditions on the platelet-like and the spherical-shaped washed samples (Figure 5). Such a significant photoactivity improvement should result from multiple positive effects related to the titania crystal morphology.

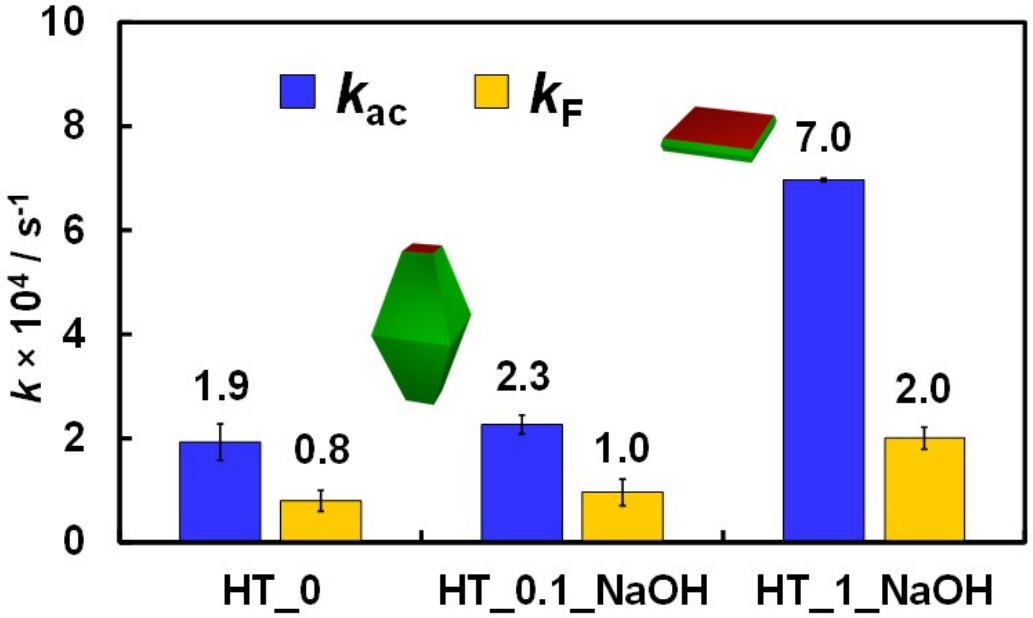

Figure 6: First order rate constants of Cr(VI) photoreduction at pH 3.7 (k_{ac}, in blue) and upon *in-situ* fluorination at the same pH (k_F, in yellow).

In fact, a significant enhancement in the effective photogenerated charge carrier separation may be attained with increasing the {001} facets exposure in TiO_2, leading to platelet-like better performing materials [58,67–69].

Interestingly, anatase crystals with different co-exposed facets can be envisaged forming 'surface heterojunctions' [58,67,70], with the selective migration of photogenerated holes and electrons towards {001} and {101} facets, respectively, being driven by the minimization of their respective energies. In particular, an optimal percent mixture of different anatase facets might have positive effects in electron-hole pair separation, as in mixed anatase-rutile systems [71]. Of course, the optimal percent amount of exposed {001} facets in anatase materials, *i.e.* ensuring the highest photoactivity, depends on the relative rates of the two simultaneous (reduction and oxidation) semi-reactions involved in the overall investigated photocatalytic

process, the best charge carrier separation being generally gained for anatase samples with ca. 50-60% of {001} facets content. Interestingly, He *et al*. [22] reported a maximum photoactivity in Cr(VI) reduction for TiO_2 materials showing a percent amount of {001} facets equal to 72%, which is comparable to the {001} facets exposure of the here investigated best performing HT_1_NaOH sample. This confirm that a balanced exposure of {001} and {101} facets is needed to achieve an optimal distribution of electrons and holes between them, *i.e.* possibly depending on the peculiar investigated substrate-sensitive process [58].

In addition, the overall efficiency of photocatalytic processes is generally affected by the extent and mode of substrate adsorption, which may also depend on the type of crystal facets predominantly exposed by the anatase photocatalyst, since facets differ in their surface atomic structure [72,73].

In the specific case of Cr(VI) photocatalytic reduction, {001} facets, displaying 100% unsaturated surface Ti-5c and undercoordinated O-2c atoms, tend to favour the dissociative adsorption/chemisorption of water (or methanol) molecules, accompanied by the formation of terminal Ti−OH species [74,75], possibly in a larger extent under irradiation conditions. Such TiO_2 surface bound -OH moieties may thus behave as crucial adsorption sites for promoting fast and efficient dichromate anions adsorption [30,63], resulting in their faster conversion to Cr(III) through their direct interaction with electrons photopromoted in the TiO_2 conduction band [65]. The presence of a relatively high amount of {001} facets may be necessary in order to promote the overall water oxidation semi-reaction, with a consequent beneficial effect also on the simultaneous photocatalytic Cr(VI) photocatalytic reduction process.

The combination of both electronic and adsorption effects, therefore, may lead to higher rate of dichromate photoreduction on the {001}-facet enriched TiO_2 material, highlighting a TiO_2 facet-dependent photoactivity in the photocatalytic degradation of Cr(VI).

Regardless of the specific TiO_2 morphology, *in-situ* surface fluorination of washed samples leads to a conspicuous (*ca.* 60-70%) photoactivity decrease, most probably consequent to a dramatically reduced adsorption of negatively charged $Cr_2O_7^{2-}$ ions (Fig. 5). This confirms the major role played by the specific substrate-TiO_2 interactions on the overall efficiency of Cr(VI) photocatalytic reduction. However, the photoactivity decrease, though being clearly evident, is not as strong as the *ca*. 90% surface substrate adsorption inhibition effect induced by *in-situ* fluorination (Figure 4). This finding results to be in line with a previous research carried out by Ku *et al.* [30], in which the pH effect on the photocatalytic reduction of Cr(VI) was found to behave differently from the Cr(VI) adsorption capability on TiO_2 surface. So, though being fundamental, the TiO_2 adsorption capability towards dichromate anions does not represent the only parameter directly influencing the rate determining step of Cr(VI) photoreduction, *i.e.* the overall photocatalytic process being also affected by the photogenerated electrons transfer towards dichromate anions, occurring afterwards the adsorption step.

3.3 Rhodamine B adsorption and photocatalytic oxidation

The relative percent amounts of RhB adsorbed on the pseudo-spherical and platelet-like shaped materials (*i.e.* HT_0.1_NaOH and HT_1_NaOH, respectively) during adsorption tests performed at pH 3.7 (blue) and at this pH in the presence of fluoride anions, with a F/Ti ratio corresponding to 2 (yellow), are reported in Figure 7.

The adsorption of the cationic dye on TiO_2 surface at pH 3.7 is rather poor and further inhibited by *in-situ* fluorination of TiO_2, most likely due to alterations of the adsorption equilibrium at the water-TiO_2 interface induced upon substitution of $\equiv Ti-OH$ terminal groups with $\equiv Ti-F$ moieties, in line with previous findings achieved for other organic dyes [66,76]. The adsorption of the organic substrate seems to be slightly hindered by a platelet-like TiO_2 morphology and this effect is maintained upon *in-situ* fluorination the TiO_2 surface. In fact, as evidenced in Fig. 7 the relative percent amounts of adsorbed RhB decreased of *ca.* 76%

and 66%, upon fluoride ions addition, for the HT_1_NaOH and the HT_0.1_NaOH samples, respectively. This finding may indirectly suggest a more extensive {001} surface coverage with fluorinated sites, thus accompanied by a more marked RhB surface adsorption inhibition.

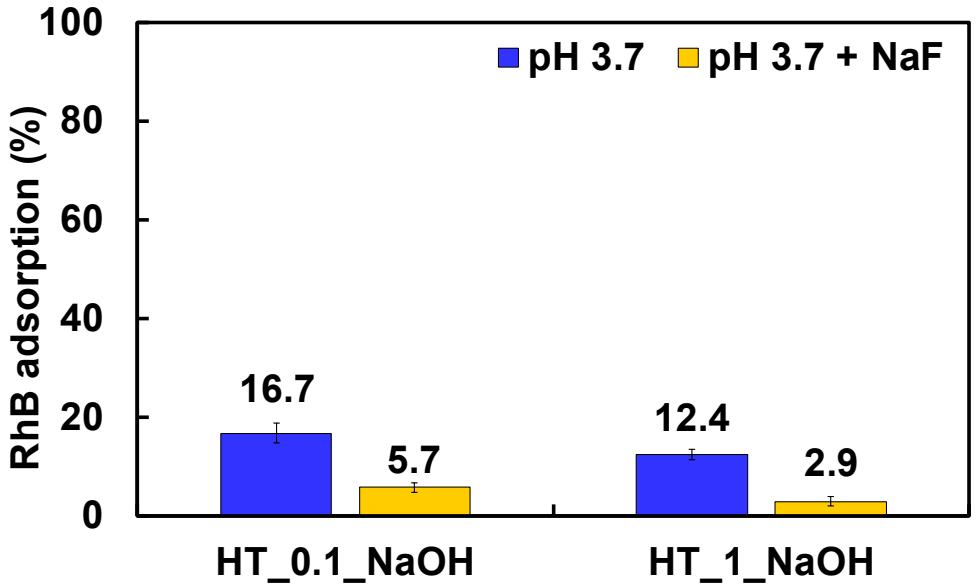

Figure 7: Percent amounts of adsorbed RhB on HT_0.1_NaOH and HT_1_NaOH after 180 min stirring in the dark in the absence of fluoride at acidic pH (blue) and at acidic pH in the presence of a F/Ti ratio in aqueous suspension equal to 2 (yellow).

Firstly, in order to check that RhB photobleaching occurs thorough the photocatalytic path (and not through self-degradation), the photostability of Rhodamine B was confirmed by 6-hours long experiments at pH 3.7, both in the absence and in the presence of fluoride anions, under the here adopted UV-vis light irradiation.

The photocatalytic degradation of Rhodamine B always occurred according to a first-order kinetics. The intensity of the RhB maximum absorption at 553 nm always gradually decreased during the runs, with a very limited hypsochromic shift in the absorption spectrum, without the appearance of any other absorption features (see Figure 8a). This excludes the formation of high concentration of light absorbing species during the runs. Consequently, the absorbance values at 553 nm can be taken as only due to RhB absorption.

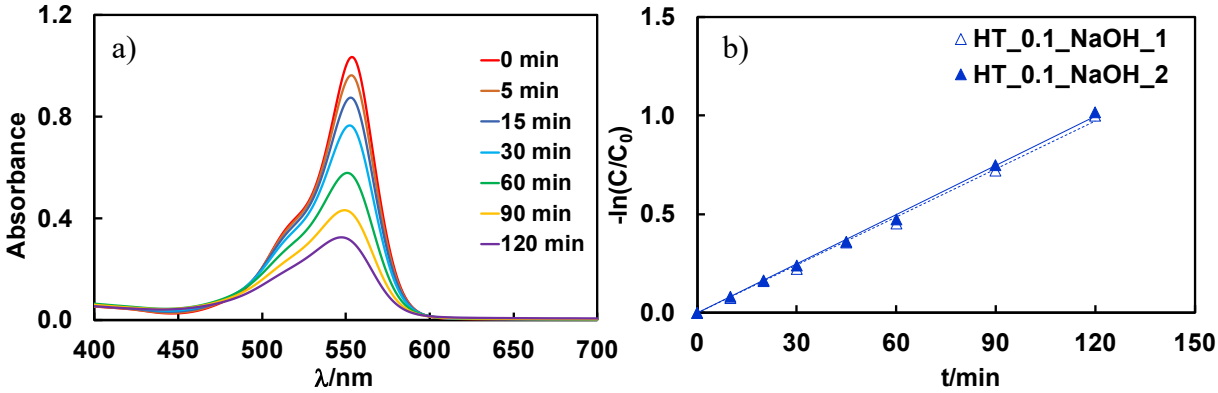

Figure 8: (a) RhB absorption spectra recorded during its photocatalytic degradation in aqueous suspension at pH 3.7 on the HT_0.1_NaOH and b) data elaboration according to first – order plots obtained in two runs under identical conditions.

This finding, in line with data reported in the literature [31,77,78], supported the idea that the RhB oxidative degradation mainly proceeded through the cleavage of the RhB chromophore group, which may occur 1) via the direct interaction of RhB molecules with positive valence band holes (h_{VB}^{+}) photogenerated on the semiconductor surface or 2) through the indirect, *i.e.* •OH radicals-mediated, degradation mechanism/path.

The photoactivity trend of the home-made photocatalysts in RhB bleaching is shown in Figure 9, in terms of first order rate constants, determined in aqueous suspensions at natural pH (k_{nat}), or measured at pH 3.7 in the absence (k_{ac}) or in the presence of fluoride ions (*in-situ* fluorinated surface, k_F).

The photoefficiency shown by the plate-like sample at natural or acidic pH are quite similar to those attained with the samples mainly exposing {101} facets, *i.e.* the specific TiO_2 morphology does not significantly affect RhB photodegradation, differently from what observed in the case of Cr(VI) photoreduction. Moreover, while lowering the pH has a negligible effect on the reaction rate, the *in-situ* fluorination is beneficial, although it hinders RhB surface adsorption.

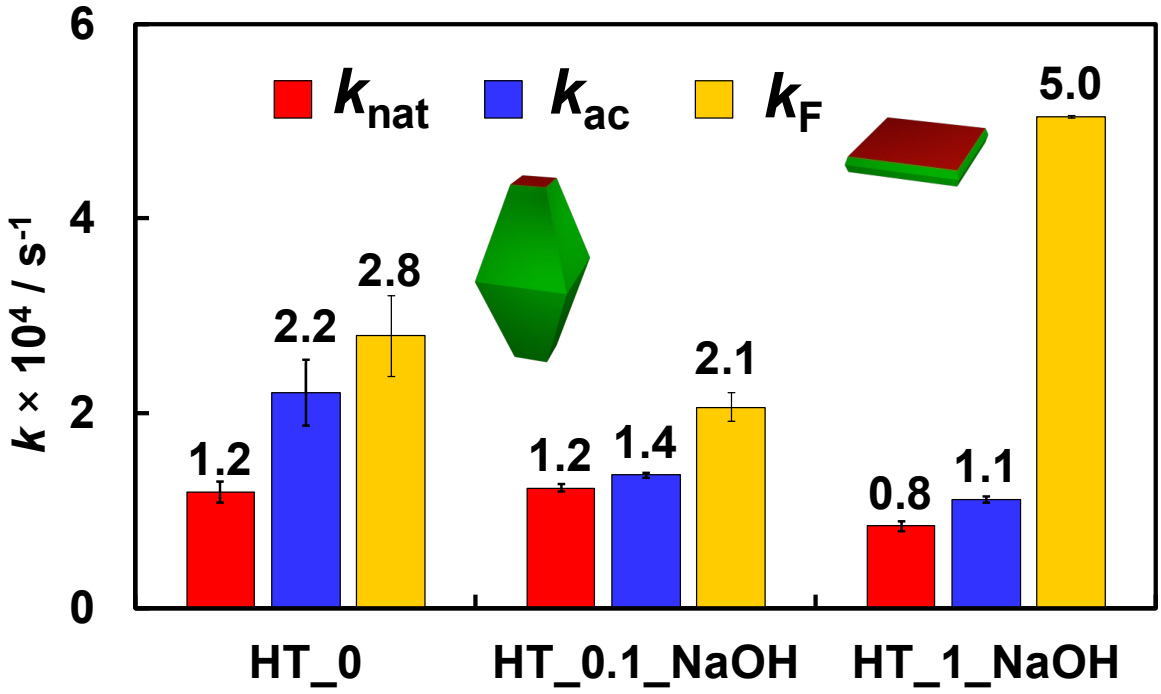

Figure 9: First-order rate constants k of RhB photodegradation for the HT series samples in the absence of fluorides at natural pH (red, k_{nat}), at acidic pH (blue, k_{ac}) or at acidic pH in the presence of a F/Ti ratio equal to 2 (yellow, k_F).

Due to the relatively poor RhB adsorption on the investigated materials surface, it is likely to expect that, differently from Cr(VI) photoreduction, a direct reaction mechanism occurring between the positive valence band holes (h_{VB}^+) photogenerated on the photocatalyst surface and the adsorbed substrate molecules cannot be envisaged as the main RhB photobleaching path. The interaction of the dye molecules with hydroxyl radicals, formed upon h_{VB}^+-induced oxidation of water molecules, may play a more important role on the overall photocatalytic degradation mechanism of the organic substrate, especially in the case of *in-situ* fluorinated TiO_2 materials, for which the RhB surface adsorption capability resulted to be extremely inhibited/hindered (Figure 7).

In this context, an increase in RhB degradation rate upon TiO_2 surface fluorination can only be explained by considering an enhanced photoproduction of $^{\bullet}OH$ radicals, which may attack the RhB molecules, thus promoting their photodegradation [31,32,79]. In fact, fluoride ions

substituting for TiO_2 surface –OH groups inhibit surface trapping of photogenerated holes as ≡Ti-O$^{\bullet}$ species, through the following reaction;

$$\equiv \mathrm{Ti} - \mathrm{OH} + \mathrm{h}_{vb}^{+} \rightarrow \equiv \mathrm{Ti} - \mathrm{O}^{\cdot} + \mathrm{H}^{+} \quad (2)$$

At the same time, by considering that $\equiv \mathrm{Ti} - \mathrm{F}$ species are stable and cannot be oxidized by valence band holes even at the here employed acidic pH [76], surface –F ions favour the desorption of photogenerated active species, *i.e.* $^{\bullet}$OH free radicals, which can thus accumulate in the aqueous phase [80], as follows:

$$\equiv \mathrm{Ti} - \mathrm{F} + \mathrm{h}_{vb}^{+} + \mathrm{H_2O} \rightarrow \equiv \mathrm{Ti} - \mathrm{F} + \mathrm{HO}^{\cdot} + \mathrm{H}^{+} \quad (3)$$

In particular, an outstanding photoactivity increase is observed upon surface fluorination of the {001}-facet enriched HT_1_NaOH sample, with a k_F/k_{ac} ratio of 4.52 (see Table 3). Thus, a clear synergistic effect induced by the plate-like anatase TiO_2 morphology and its *in-situ* surface fluorination is clearly outlined in RhB degradation. Moreover, as reported in Table 3, similar k_F/k_{ac} ratios were obtained for both HT_1_NaOH and HT_1, which were significantly higher than the k_F/k_{ac} ratios obtained for the HT_0.1_NaOH and HT_0.1. This provides a further confirmation of the here unveiled synergistic effect.

In particular, the absence of any significant morphology-dependent RhB adsorption effect on fluorinated TiO_2 surfaces suggests that such rate increase is related to the intrinsic ability of F-{001} facets of boosting $^{\bullet}$OH radical mediated oxidation paths, possibly due to an improved charge carriers separation. A cooperative contribution in improving the separation of photogenerated charge carriers upon fluorination of {001}-facet enriched materials may be at the origin of the here observed morphology-dependent synergistic effect, as previously reported by Chen *et al*. for the gas phase photocatalytic oxidation of ammonia [81]. The spontaneous tendency of photogenerated holes to migrate towards {001} facets [58,67,68] is amplified by the electric-field effect induced by fluorination [82], *i.e.* promoting holes attraction towards {001} facets (present in larger extent) and photogenerated electrons

repulsion towards {101} facets, with a consequent overall beneficial increase of photogenerated charge carriers separation.

Table 3: Ratios between the rate constants of RhB photodegradation performed under different experimental conditions.

Sample	k_{ac} / k_{nat}	k_F / k_{ac}
HT_0	1.86 ± 0.33	1.26 ± 0.27
HT_0.1_NaOH	1.11 ± 0.04	1.51 ± 0.11
HT_1_NaOH	1.33 ± 0.09	4.52 ± 0.15
HT_0.1	1.41 ± 0.10	1.42 ± 0.22
HT_1	1.22 ± 0.12	4.94 ± 0.02

Moreover, the beneficial effect of surface fluorination on the photoactivity of plate-like TiO_2 in RhB degradation may originate from the presence of specific surface defects and/or the enhanced initial exposure of surface OH groups [74] (due to favored water molecules dissociation), leading then to a higher surface density of fluorinated sites, which are involved in the production and release/accumulation of reactive $^{\bullet}OH$ radicals, as discussed above.

In order to get better insight at the molecular level into the differences in surface hydration and hydroxylation between HT_0.1_NaOH and HT_1_NaOH, we employed FT-IR spectroscopy. From the black spectra in Figure 10, obtained after outgassing at room temperature, we can observe that both samples show an evident band at 1620 cm^{-1}, ascribed to $\delta(H_2O)$, *i.e.* bending mode of adsorbed water [74]. The H_2O molecules are not isolated, but are interacting by hydrogen bond as testified by the intense and broad ν(OH) band in the 3600-3000 cm^{-1} range [83]. In this spectral region also the IR signals of OH groups are present, but to properly investigate them it is necessary to remove molecular water by outgassing at increasing temperatures. Heating at 150 °C (blue curves in Figure 10) considerably decreases the intensity of the $\delta(H_2O)$ band, which finally disappears at 300 °C (grey curves in Figure 10), i.e. molecular water being completely removed from both samples by outgassing at such temperature. Interestingly, considering the grey spectra in the ν(OH) spectral region, we can

note that HT_0.1_NaOH shows only some weak and sharp components at $\nu \geq 3600$ cm^{-1} due to few isolated OH groups [75,84]. Conversely, HT_1_NaOH still exhibits a broad and quite intense band in the 3600-3000 cm^{-1} range, arising from a significant number of hydroxyls still present on the {001} facets, which are expected to strongly adsorb water in a dissociative way [52,85]. Finally, outgassing at 500 °C (red curves in Figure 10) nearly completely removes the OH groups from both samples. The IR results thus confirm that plate-like TiO_2 shows a considerably higher concentration of OH groups that can be fluorinated and lead to a significantly enhanced production of hydroxyl radicals, which are considered as the main oxygen reactive species involved in the photocatalytic oxidation of Rhodamine B molecules.

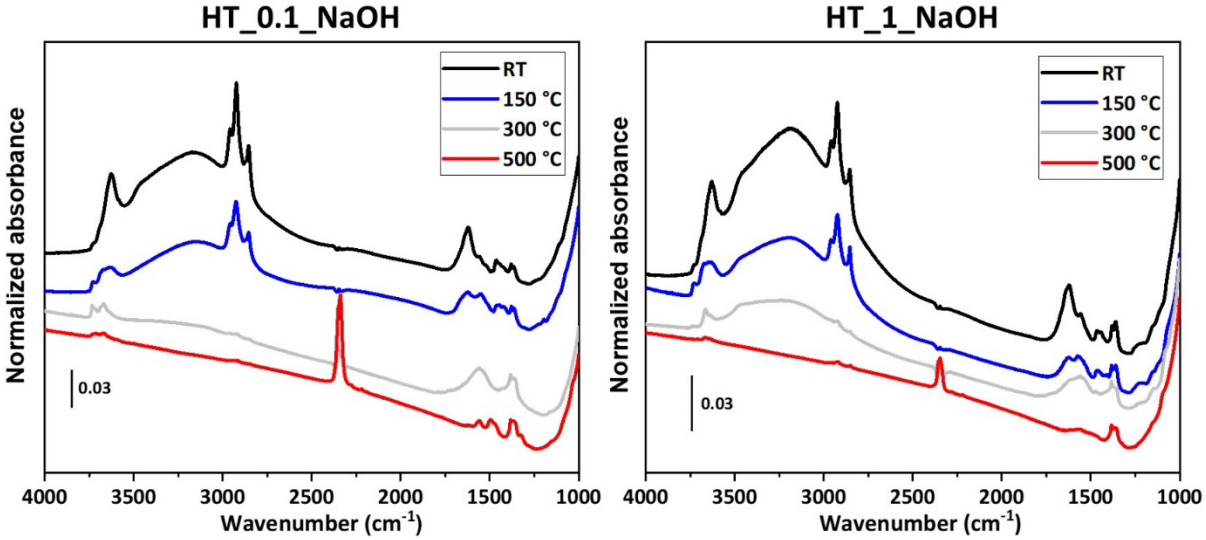

Figure 10: FT-IR spectra of the HT_0.1_NaOH and HT_1_NaOH samples outgassed for 1 hour at increasing temperatures: room temperature (black curve), 150 °C (blue curve), 300 °C (grey curve) and 500 °C (red curve).

4 CONCLUSIONS

In the present study we shed light on the effects deriving from combining *in-situ* surface fluorination and morphology control in a reduction and an oxidation photocatalytic test reactions. Cr(VI) photoreduction is strongly favored by a larger exposure of {001} facets, with the best performing material having a platelet-like morphology, possibly due to improved charge separation arising from an optimal mixture of co-exposed facets, favouring the selective

migration of photogenerated holes and electrons towards {001} and {101} facets, respectively. *In-situ* re-fluorination of the material surface, however, led to a morphology independent photoactivity decrease, consequent to the reduced ability of the fluorinated oxide to bind dichromate anions, a key step necessary for their direct reduction by means of CB electrons.

A strong synergistic shape-dependent photoactivity effect between plate-like anatase TiO_2 morphology and surface fluorination has been clearly outlined in Rhodamine B photodegradation, with an outstanding photoactivity increase observed only upon fluorination of {001}-facet enriched materials. This most likely results from the higher concentration of OH groups in the plate-like TiO_2 that can be fluorinated to generate F-{001} facets, which may considerably boost $^{\bullet}OH$ radical mediated oxidation paths.

The here unveiled role played by morphology and surface fluorination on the photoactivity of shape-controlled TiO_2 materials may pave the way for designing highly performant TiO_2-based materials to be employed in efficient photocatalytic detoxification processes.

Acknowledgements

The collaboration of Dr. Adele Scaltrini in performing photocatalytic oxidation/reduction kinetic runs and of Dr. Erica Montanari in carrying out HR-TEM measurements is gratefully acknowledged. This work received financial support from the University of Milano PSR2020_DIP_005_PI_MDOZZ project "Piano di Sostegno alla Ricerca 2020, linea 2, Azione A".

TOC

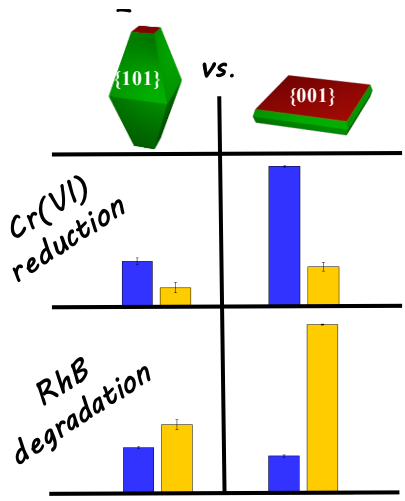

Highlights

- Both plate-like (PL) and spherical shape anatase TiO_2 samples are prepared
- Effects induced on photoactivity by TiO_2 shape and surface fluorination (SF) are studied
- Cr(VI) photoreduction (PR) is strongly favored by a larger exposure of {001} facets
- In-situ TiO_2 SF leads to a systematic and morphology independent Cr(VI) PR decrease
- Beneficial synergistic effect of PL morphology and SF is outlined in RhB degradation

REFERENCES

[1] X. Zhou, N. Liu, P. Schmuki, Photocatalysis with TiO_2 Nanotubes: "Colorful" Reactivity and Designing Site-Specific Photocatalytic Centers into TiO_2 Nanotubes, ACS Catal. 7 (2017) 3210–3235. doi:10.1021/acscatal.6b03709.

[2] S. Wang, Z. Ding, X. Chang, J. Xu, D.-H. Wang, Modified Nano-TiO_2 Based Composites for Environmental Photocatalytic Applications, Catalysts. 10 (2020) 1–38.

[3] M. Gao, L. Zhu, W.L. Ong, J. Wang, G.W. Ho, Structural design of TiO_2-based photocatalyst for H_2 production and degradation applications, Catal. Sci. Technol. 5 (2015) 4703–4726. doi:10.1039/C5CY00879D.

[4] S.B. Patil, P.S. Basavarajappa, N. Ganganagappa, M.S. Jyothi, A.V. Raghu, K.R. Reddy, Recent advances in non-metals-doped TiO_2 nanostructured photocatalysts for visible-light driven hydrogen production, CO_2 reduction and air purification, Int. J. Hydrogen Energy. 44 (2019) 13022–13039. doi:10.1016/j.ijhydene.2019.03.164.

[5] A. Mittal, B. Mari, S. Sharma, V. Kumari, S. Maken, K. Kumari, N. Kumar, Non-metal modified TiO_2: a step towards visible light photocatalysis, J. Mater. Sci. Mater. Electron. 30 (2019) 3186–3207. doi:10.1007/s10854-018-00651-9.

[6] A. Truppi, F. Petronella, T. Placido, M. Striccoli, A. Agostiano, M. Curri, R. Comparelli, Visible-Light-Active TiO_2-Based Hybrid Nanocatalysts for Environmental Applications, Catalysts. 7 (2017) 100–1/33. doi:10.3390/catal7040100.

[7] S. Bera, D. Il Won, S.B. Rawal, H.J. Kang, W.I. Lee, Design of visible-light photocatalysts by coupling of inorganic semiconductors, Catal. Today. 335 (2019) 3–19. doi:10.1016/j.cattod.2018.11.001.

[8] H. Xu, S. Ouyang, L. Liu, P. Reunchan, N. Umezawa, J. Ye, Recent advances in TiO2-based photocatalysis, J. Mater. Chem. A. 2 (2014) 12642–12661. doi:10.1039/C4TA00941J.

[9] G. Li, K.A. Gray, The solid–solid interface: Explaining the high and unique photocatalytic reactivity of TiO_2-based nanocomposite materials, Chem. Phys. 339 (2007) 173–187. doi:10.1016/j.chemphys.2007.05.023.

[10] S.G. Kumar, K.S.R.K. Rao, Comparison of modification strategies towards enhanced charge carrier separation and photocatalytic degradation activity of metal oxide semiconductors (TiO_2, WO_3 and ZnO), Appl. Surf. Sci. 391 (2017) 124–148. doi:10.1016/j.apsusc.2016.07.081.

[11] G. Liu, J.C. Yu, G.Q. (Max) Lu, H.-M. Cheng, Crystal facet engineering of semiconductor photocatalysts: motivations, advances and unique properties, Chem. Commun. 47 (2011) 6763–6783. doi:10.1039/c1cc10665a.

[12] W.-J. Ong, L.-L. Tan, S.-P. Chai, S.-T. Yong, A.R. Mohamed, Highly reactive {001} facets of TiO_2-based composites: synthesis, formation mechanism and characterization, Nanoscale. 6 (2014) 1946–2008. doi:10.1039/c3nr04655a.

[13] M.V. Dozzi, E. Selli, Specific Facets-Dominated Anatase TiO_2: Fluorine-Mediated Synthesis and Photoactivity, Catalysts. 3 (2013) 455–485. doi:10.3390/catal3020455.

[14] K. Wang, M. Janczarek, Z. Wei, T. Raja-Mogan, M. Endo-Kimura, T.M. Khedr, B. Ohtani, E. Kowalska, Morphology-and crystalline composition-governed activity of titania-based photocatalysts: Overview and perspective, Catalysts. 9 (2019) 1054–1/30. doi:10.3390/catal9121054.

[15] M. Maisano, M.V. Dozzi, E. Selli, Searching for facet-dependent photoactivity of shape-controlled anatase TiO_2, J. Photochem. Photobiol. C Photochem. Rev. 28 (2016) 29–43. doi:10.1016/j.jphotochemrev.2016.07.002.

[16] K. Lv, X. Li, K. Deng, J. Sun, X. Li, M. Li, Effect of phase structures on the photocatalytic activity of surface fluorinated TiO_2, Appl. Catal. B Environ. 95 (2010) 383–392. doi:10.1016/j.apcatb.2010.01.017.

[17] W. Choi, Pure and modified TiO_2 photocatalysts and their environmental applications, Catal. Surv. from Asia. 10 (2006) 16–28. doi:10.1007/s10563-006-9000-2.

[18] C. Minero, G. Mariella, V. Maurino, E. Pelizzetti, Photocatalytic Transformation of Organic Compounds in the Presence of Inorganic Anions. 1. Hydroxyl-Mediated and Direct Electron-Transfer Reactions of Phenol on a Titanium Dioxide−Fluoride System, Langmuir. 16 (2000) 2632–2641. doi:10.1021/la9903301.

[19] J. Kim, W. Choi, H. Park, Effects of TiO_2 surface fluorination on photocatalytic degradation of methylene blue and humic acid, Res. Chem. Intermed. 36 (2010) 127–140. doi:10.1007/s11164-010-0123-8.

[20] M. Mrowetz, E. Selli, H_2O_2 evolution during the photocatalytic degradation of organic molecules on fluorinated TiO_2, New J. Chem. 30 (2006) 108–114. doi:10.1039/B511320B.

[21] M.V. Dozzi, E. Selli, Effects of phase composition and surface area on the photocatalytic paths on fluorinated titania, Catal. Today. 206 (2013) 26–31. doi:10.1016/j.cattod.2012.03.029.

[22] Z. He, Q. Cai, M. Wu, Y. Shi, H. Fang, L. Li, J. Chen, J. Chen, S. Song, Photocatalytic Reduction of Cr(VI) in an Aqueous Suspension of Surface-Fluorinated Anatase TiO_2 Nanosheets with Exposed {001} Facets, Ind. Eng. Chem. Res. 52 (2013) 9556–9565. doi:10.1021/ie400812m.

[23] X. Li, J. Zhu, H. Li, Influence of crystal facets and F-modification on the photocatalytic performance of anatase TiO_2, Catal. Commun. 24 (2012) 20–24. doi:10.1016/j.catcom.2012.03.009.

[24] Z. He, L. Jiang, D. Wang, J. Qiu, J. Chen, S. Song, Simultaneous Oxidation of p-Chlorophenol and Reduction of Cr(VI) on Fluorinated Anatase TiO_2 Nanosheets with Dominant {001} Facets under Visible Irradiation, Ind. Eng. Chem. Res. 54 (2015) 808–818. doi:10.1021/ie503997m.

[25] H. Wu, J. Ma, Y. Li, C. Zhang, H. He, Photocatalytic oxidation of gaseous ammonia over fluorinated TiO_2 with exposed (001) facets, Appl. Catal. B Environ. 152–153 (2014) 82–87. doi:10.1016/j.apcatb.2014.01.021.

[26] P. Mikrut, M. Kobielusz, W. Macyk, Spectroelectrochemical characterization of euhedral anatase TiO_2 crystals – Implications for photoelectrochemical and photocatalytic properties of {001} {100} and {101} facets, Electrochim. Acta. 310 (2019) 256–265. doi:10.1016/j.electacta.2019.04.043.

[27] Q. Xiang, K. Lv, J. Yu, Pivotal role of fluorine in enhanced photocatalytic activity of anatase TiO_2 nanosheets with dominant (001) facets for the photocatalytic degradation of acetone in air, Appl. Catal. B Environ. 96 (2010) 557–564. doi:10.1016/j.apcatb.2010.03.020.

[28] K. Lv, Q. Xiang, J. Yu, Effect of calcination temperature on morphology and

photocatalytic activity of anatase TiO_2 nanosheets with exposed {001} facets, Appl. Catal. B Environ. 104 (2011) 275–281. doi:10.1016/j.apcatb.2011.03.019.

[29] M. Maisano, M.V. Dozzi, M. Coduri, L. Artiglia, G. Granozzi, E. Selli, Unraveling the Multiple Effects Originating the Increased Oxidative Photoactivity of {001}-Facet Enriched Anatase TiO_2, ACS Appl. Mater. Interfaces. 8 (2016) 9745−9754. doi:10.1021/acsami.6b01808.

[30] Y. Ku, I.-L. Jung, Photocatalytic reduction of Cr(VI) in aqueous solutions by UV irradiation with the presence of titanium dioxide, Water Res. 35 (2001) 135–142. doi:10.1016/S0043-1354(00)00098-1.

[31] P. Qu, J. Zhao, T. Shen, H. Hidaka, TiO_2-assisted photodegradation of dyes: A study of two competitive primary processes in the degradation of RB in an aqueous TiO_2 colloidal solution, J. Mol. Catal. A Chem. 129 (1998) 257–268. doi:10.1016/S1381-1169(97)00185-4.

[32] L. Qi, J. Yu, M. Jaroniec, Enhanced and suppressed effects of ionic liquid on the photocatalytic activity of TiO_2, Adsorption. 19 (2013) 557–561. doi:10.1007/s10450-013-9478-7.

[33] J. Ke, M. Adnan Younis, Y. Kong, H. Zhou, J. Liu, L. Lei, Y. Hou, Nanostructured Ternary Metal Tungstate-Based Photocatalysts for Environmental Purification and Solar Water Splitting: A Review, Nano-Micro Lett. 10 (2018) 1–27. doi:10.1007/s40820-018-0222-4.

[34] H. Park, Y. Park, W. Kim, W. Choi, Surface modification of TiO_2 photocatalyst for environmental applications, J. Photochem. Photobiol. C Photochem. Rev. 15 (2013) 1–20. doi:10.1016/j.jphotochemrev.2012.10.001.

[35] Y.H. Chiu, T.F.M. Chang, C.Y. Chen, M. Sone, Y.J. Hsu, Mechanistic insights into photodegradation of organic dyes using heterostructure photocatalysts, Catalysts. 9 (2019) 430–1/32. doi:10.3390/catal9050430.

[36] M.V. Dozzi, A. Saccomanni, E. Selli, Cr(VI) photocatalytic reduction: Effects of simultaneous organics oxidation and of gold nanoparticles photodeposition on TiO_2, J. Hazard. Mater. 211 (2012) 188–195. doi:10.1016/j.jhazmat.2011.09.038.

[37] Y.-X. Li, X. Wang, C.-C. Wang, H. Fu, Y. Liu, P. Wang, C. Zhao, S-TiO_2/UiO-66-NH_2 composite for boosted photocatalytic Cr(VI) reduction and bisphenol A degradation under LED visible light, J. Hazard. Mater. 399 (2020) 123085–1/14. doi:10.1016/j.jhazmat.2020.123085.

[38] Y.X. Li, H. Fu, P. Wang, C. Zhao, W. Liu, C.C. Wang, Porous tube-like ZnS derived from rod-like ZIF-L for photocatalytic Cr(VI) reduction and organic pollutants degradation, Environ. Pollut. 256 (2020) 113417–1/13. doi:10.1016/j.envpol.2019.113417.

[39] C.D. Palmer, P.R. Wittbrodt, Processes affecting the remediation of chromium-contaminated sites., Environ. Health Perspect. 92 (1991) 25–40. doi:10.1289/ehp.919225.

[40] V. Bianchi, A. Zantedeschi, A. Montaldi, F. Majone, Trivalent chromium is neither cytotoxic nor mutagenic in permeabilized hamster fibroblasts, Toxicol. Lett. 23 (1984) 51–59. doi:10.1016/0378-4274(84)90009-2.

[41] Y.Y. Cheng, T.H. Tsai, Pharmacokinetics and Biodistribution of the Illegal Food

Colorant Rhodamine B in Rats, J. Agric. Food Chem. 65 (2017) 1078–1085. doi:10.1021/acs.jafc.6b04975.

[42] L. Spessato, V.A. Duarte, P. Viero, H. Zanella, J.M. Fonseca, P.A. Arroyo, V.C. Almeida, Optimization of Sibipiruna activated carbon preparation by simplex-centroid mixture design for simultaneous adsorption of rhodamine B and metformin, J. Hazard. Mater. 411 (2021) 125166–1/16. doi:10.1016/j.jhazmat.2021.125166.

[43] J.S. Chen, X.W. Lou, Anatase TiO_2 nanosheet: An ideal host structure for fast and efficient lithium insertion/extraction, Electrochem. Commun. 11 (2009) 2332–2335. doi:10.1016/j.elecom.2009.10.024.

[44] H. Wu, J. Ma, Y. Li, C. Zhang, H. He, Photocatalytic oxidation of gaseous ammonia over fluorinated TiO_2 with exposed (001) facets, Appl. Catal. B Environ. 152–153 (2014) 82–87. doi:10.1016/j.apcatb.2014.01.021.

[45] M. Coduri, M. Maisano, M.V. Dozzi, E. Selli, Morphological characterization of shape-controlled TiO_2 anatase through XRPD analysis, Zeitschrift Fur Phys. Chemie. 230 (2016) 1233–1248. doi:10.1515/zpch-2015-0715.

[46] A. Altomare, M.C. Burla, C. Giacovazzo, A. Guagliardi, A.G.G. Moliterni, G. Polidori, R. Rizzi, Quanto : a Rietveld program for quantitative phase analysis of polycrystalline mixtures, J. Appl. Crystallogr. 34 (2001) 392–397. doi:10.1107/S0021889801002904.

[47] M. Abdullah, G.K.C. Low, R.W. Matthews, Effects of common inorganic anions on rates of photocatalytic oxidation of organic carbon over illuminated titanium dioxide, J. Phys. Chem. 94 (1990) 6820–6825. doi:10.1021/j100380a051.

[48] L.S. Clesceri, A.E. Greenberg, A.D. Eaton, Standard Methods for the Examination of Water and Wastewater, 20th Ed., 1998.

[49] X. Wang, S.O. Pehkonen, A.K. Ray, Removal of Aqueous Cr(VI) by a Combination of Photocatalytic Reduction and Coprecipitation, Ind. Eng. Chem. Res. 43 (2004) 1665–1672. doi:10.1021/ie030580j.

[50] C. Bernardini, G. Cappelletti, M.V. Dozzi, E. Selli, Photocatalytic degradation of organic molecules in water: Photoactivity and reaction paths in relation to TiO_2 particles features, J. Photochem. Photobiol. A Chem. 211 (2010) 185–192. doi:10.1016/j.jphotochem.2010.03.006.

[51] H.M. Rietveld, A profile refinement method for nuclear and magnetic structures, J. Appl. Crystallogr. 2 (1969) 65–71. doi:10.1107/S0021889869006558.

[52] L. Mino, F. Pellegrino, S. Rades, J. Radnik, V.D. Hodoroaba, G. Spoto, V. Maurino, G. Martra, Beyond Shape Engineering of TiO_2 Nanoparticles: Post-Synthesis Treatment Dependence of Surface Hydration, Hydroxylation, Lewis Acidity and Photocatalytic Activity of TiO_2 Anatase Nanoparticles with Dominant {001} or {101} Facets, ACS Appl. Nano Mater. 1 (2018) 5355–5365. doi:10.1021/acsanm.8b01477.

[53] L. Ye, J. Mao, J. Liu, Z. Jiang, T. Peng, L. Zan, Synthesis of anatase TiO_2 nanocrystals with {101}, {001} or {010} single facets of 90% level exposure and liquid-phase photocatalytic reduction and oxidation activity orders, J. Mater. Chem. A. 1 (2013) 10532–10537. doi:10.1039/c3ta11791j.

[54] L. Liu, Z. Liu, A. Liu, X. Gu, C. Ge, F. Gao, L. Dong, Engineering the TiO_2-graphene interface to enhance photocatalytic H_2 production, ChemSusChem. 7 (2014) 618–626. doi:10.1002/cssc.201300941.

[55] T. Li, B. Tian, J. Zhang, R. Dong, T. Wang, F. Yang, Facile tailoring of anatase TiO_2 morphology by use of H_2O_2: From microflowers with dominant {101} facets to microspheres with exposed {001} facets, Ind. Eng. Chem. Res. 52 (2013) 6704–6712. doi:10.1021/ie3030714.

[56] Y. Luan, L. Jing, Y. Xie, X. Sun, Y. Feng, H. Fu, Exceptional photocatalytic activity of 001-facet-exposed TiO_2 mainly depending on enhanced adsorbed oxygen by residual hydrogen fluoride, ACS Catal. 3 (2013) 1378–1385. doi:10.1021/cs400216a.

[57] C. Li, C. Koenigsmann, W. Ding, B. Rudshteyn, K.R. Yang, K.P. Regan, S.J. Konezny, V.S. Batista, G.W. Brudvig, C.A. Schmuttenmaer, J.-H. Kim, Facet-Dependent Photoelectrochemical Performance of TiO_2 Nanostructures: An Experimental and Computational Study, J. Am. Chem. Soc. 137 (2015) 1520–1529. doi:10.1021/ja5111078.

[58] J. Yu, J. Low, W. Xiao, P. Zhou, M. Jaroniec, Enhanced Photocatalytic CO_2-Reduction Activity of Anatase TiO_2 by Coexposed {001} and {101} Facets, J. Am. Chem. Soc. 136 (2014) 8839–8842. doi:10.1021/ja5044787.

[59] M. Bernareggi, M.V. Dozzi, L. Bettini, A. Ferretti, G. Chiarello, E. Selli, Flame-Made Cu/TiO_2 and $Cu-Pt/TiO_2$ Photocatalysts for Hydrogen Production, Catalysts. 7 (2017) 301–1/14. doi:10.3390/catal7100301.

[60] G. Wu, J. Wang, D.F. Thomas, A. Chen, Synthesis of F-Doped Flower-like TiO_2 Nanostructures with High Photoelectrochemical Activity, Langmuir. 24 (2008) 3503–3509. doi:10.1021/la703098g.

[61] J.C. Yu, Yu, Ho, Jiang, Zhang, Effects of F^- Doping on the Photocatalytic Activity and Microstructures of Nanocrystalline TiO_2 Powders, Chem. Mater. 14 (2002) 3808–3816. doi:10.1021/cm020027c.

[62] M.V. Dozzi, L. Artiglia, G. Granozzi, B. Ohtani, E. Selli, Photocatalytic Activity vs Structural Features of Titanium Dioxide Materials Singly Doped or Codoped with Fluorine and Boron, J. Phys. Chem. C. 118 (2014) 25579−25589.

[63] C.H. Weng, J.H. Wang, C.P. Huang, Adsorption of Cr(VI) onto TiO2 from dilute aqueous solutions, Water Sci. Technol. 35 (1997) 55–62.

[64] M. Kosmulski, The significance of the difference in the point of zero charge between rutile and anatase, Adv. Colloid Interface Sci. 99 (2002) 255–264. doi:10.1016/S0001-8686(02)00080-5.

[65] S. Asuha, X.G. Zhou, S. Zhao, Adsorption of methyl orange and Cr(VI) on mesoporous TiO_2 prepared by hydrothermal method, J. Hazard. Mater. 181 (2010) 204–210. doi:10.1016/j.jhazmat.2010.04.117.

[66] H. Park, W. Choi, Effects of TiO_2 Surface Fluorination on Photocatalytic Reactions and Photoelectrochemical Behaviors, J. Phys. Chem. B. 108 (2004) 4086–4093. doi:10.1021/jp036735i.

[67] G. Di Liberto, S. Tosoni, G. Pacchioni, Role of Heterojunction in Charge Carrier Separation in Coexposed Anatase (001)-(101) Surfaces, J. Phys. Chem. Lett. 10 (2019) 2372–2377. doi:10.1021/acs.jpclett.9b00504.

[68] T. Ohno, K. Sarukawa, M. Matsumura, Crystal faces of rutile and anatase TiO_2 particles and their roles in photocatalytic reactions, New J. Chem. 26 (2002) 1167–1170. doi:10.1039/b202140d.

[69] Z. Zheng, B. Huang, J. Lu, X. Qin, X. Zhang, Y. Dai, Hierarchical TiO_2 Microspheres: Synergetic Effect of {001} and {101} Facets for Enhanced Photocatalytic Activity, Chem. - A Eur. J. 17 (2011) 15032–15038. doi:10.1002/chem.201101466.

[70] F. Pellegrino, F. Sordello, L. Mino, C. Minero, V.D. Hodoroaba, G. Martra, V. Maurino, Formic Acid Photoreforming for Hydrogen Production on Shape-Controlled Anatase TiO_2 Nanoparticles: Assessment of the Role of Fluorides, {101}/{001} Surfaces Ratio, and Platinization, ACS Catal. 9 (2019) 6692–6697. doi:10.1021/acscatal.9b01861.

[71] P. Deák, B. Aradi, T. Frauenheim, Band Lineup and Charge Carrier Separation in Mixed Rutile-Anatase Systems, J. Phys. Chem. C. 115 (2011) 3443–3446. doi:10.1021/jp1115492.

[72] M. Lazzeri, A. Vittadini, A. Selloni, Structure and energetics of stoichiometric TiO_2 anatase surfaces, 63 (2001) 1–9. doi:10.1103/PhysRevB.63.155409.

[73] P. Zhou, H. Zhang, H. Ji, W. Ma, C. Chen, J. Zhao, Modulating the photocatalytic redox preferences between anatase TiO_2 {001} and {101} surfaces, Chem. Commun. 53 (2017) 787–790. doi:10.1039/C6CC08785J.

[74] C. Arrouvel, M. Digne, M. Breysse, H. Toulhoat, P. Raybaud, Effects of morphology on surface hydroxyl concentration: A DFT comparison of anatase-TiO_2 and γ-alumina catalytic supports, J. Catal. 222 (2004) 152–166. doi:10.1016/j.jcat.2003.10.016.

[75] L. Mino, Á. Morales-García, S.T. Bromley, F. Illas, Understanding the nature and location of hydroxyl groups on hydrated titania nanoparticles, Nanoscale. 13 (2021) 6577–6585. doi:10.1039/d1nr00610j.

[76] M. Mrowetz, E. Selli, H_2O_2 evolution during the photocatalytic degradation of organic molecules on fluorinated TiO_2, New J. Chem. 30 (2006) 108–114. doi:10.1039/b511320b.

[77] Q. Wang, C. Chen, D. Zhao, M. Wanhong, J. Zhao, Change of adsorption modes of dyes on fluorinated TiO_2 and its effect on photocatalytic degradation of dyes under visible irradiation, Langmuir. 24 (2008) 7338–7345. doi:10.1021/la800313s.

[78] C. Yao, X. Wang, W. Zhao, T. Li, Y. He, X. Ran, L. Guo, Probing the facet-dependent intermediate in the visible-light degradation of RhB by carbon-coated anatase TiO_2 nanoparticles, J. Alloys Compd. 846 (2020) 156335–1/9. doi:10.1016/j.jallcom.2020.156335.

[79] Y. Hu, D. Li, H. Wang, G. Zeng, X. Li, Y. Shao, Role of active oxygen species in the liquid-phase photocatalytic degradation of RhB using $BiVO_4$/TiO_2 heterostructure under visible light irradiation, J. Mol. Catal. A Chem. 408 (2015) 172–178. doi:10.1016/j.molcata.2015.07.025.

[80] M. Mrowetz, E. Selli, Enhanced photocatalytic formation of hydroxyl radicals on fluorinated TiO_2, Phys. Chem. Chem. Phys. 7 (2005) 1100–1102. doi:10.1039/b500194c.

[81] M. Chen, J. Ma, B. Zhang, G. He, Y. Li, C. Zhang, H. He, Remarkable synergistic effect between {001} facets and surface F ions promoting hole migration on anatase TiO_2, Appl. Catal. B Environ. 207 (2017) 397–403. doi:10.1016/j.apcatb.2017.02.048.

[82] H. Sheng, Q. Li, W. Ma, H. Ji, C. Chen, J. Zhao, Photocatalytic degradation of organic pollutants on surface anionized TiO_2: Common effect of anions for high hole-availability by water, Appl. Catal. B Environ. 138–139 (2013) 212–218.

doi:10.1016/j.apcatb.2013.03.001.

[83] L. Mino, C. Negri, R. Santalucia, G. Cerrato, G. Spoto, G. Martra, Morphology , Surface Structure and Water Adsorption Properties of TiO_2 Nanoparticles: A Comparison of Different Commercial Samples, Molecules. 25 (2020) 4605.

[84] A. Mahdavi-Shakib, J.M. Arce-Ramos, R.N. Austin, T.J. Schwartz, L.C. Grabow, B.G. Frederick, Frequencies and Thermal Stability of Isolated Surface Hydroxyls on Pyrogenic TiO_2 Nanoparticles, J. Phys. Chem. C. 123 (2019) 24533–24548. doi:10.1021/acs.jpcc.9b05699.

[85] C. Sun, L.M. Liu, A. Selloni, G.Q. Lu, S.C. Smith, Titania-water interactions: A review of theoretical studies, J. Mater. Chem. 20 (2010) 10319–10334. doi:10.1039/c0jm01491e.